Commun Nonlinear Sci Numer Simulat 17 (2012) 2052–2061

Contents lists available at SciVerse ScienceDirect

Commun Nonlinear Sci Numer Simulat

journal homepage: www.elsevier.com/locate/cnsns

Numerical study of one-dimensional Vlasov–Poisson equations for infinite homogeneous stellar systems

Yingda Cheng *, Irene M. Gamba [1]

Department of Mathematics and ICES, University of Texas at Austin, Austin, TX 78712, USA

ARTICLE INFO

Article history:
Available online 29 October 2011

Dedicated to Phil J. Morrison on his 60th birthday

Keywords:
Jeans instability
Vlasov–Poisson
Collisionless Boltzmann
Discontinuous Galerkin methods
Positivity-preserving
BGK mode

ABSTRACT

We consider the gravitational Vlasov–Poisson (VP), or the so-called collisionless Boltzmann–Poisson equations for the self-gravitating collisionless stellar systems. We compute the solutions using a high-order discontinuous Galerkin method for the Vlasov equation, and the classical representation by Green's function for the Poisson equation in the one-dimensional setting. We study both the case of damping and Jeans instability depending on the wavenumbers, which are taken to be greater than or less than the Jeans wavenumber, respectively. The method is shown to be stable, accurate and conservative. We report for the first time the BGK modes for the gravitational VP system, and we study the behavior of solutions associated with these various wavenumbers.

1. Introduction

In this paper, we consider the gravitational Vlasov–Poisson (VP), or the so-called collisionless Boltzmann–Poisson equations for the self-gravitating collisionless stellar systems. The VP system in this case describes the evolution of the density of stars in phase space and is given as follows [4],

$$\begin{aligned} &\partial_t f + v \cdot \nabla_x f + E \cdot \nabla_v f = 0 \quad \Omega \times (0,T] \\ &\Delta_x \Phi = 4\pi G \rho_0 \left(\int_{\mathbb{R}^n} f dv - 1 \right) \quad \Omega_x \times (0,T] \\ &E = -\nabla_x \Phi \quad \Omega_x \times (0,T] \end{aligned} \tag{1}$$

Here f is the stellar distribution function, G is the gravitational constant, ρ_0 is the density of the infinite homogeneous medium, E is the gravitational field, and the constant -1 in the total charge for the Poisson equation denotes the cosmological background density. The domain $\Omega = \Omega_x \times \mathbb{R}^n$, where Ω_x is the physical space and the phase space is taken to be $\mathbb{R}^n$. More detailed discussions of the above system for the galactic dynamics can be found in the book by Binney and Tremaine [4].

There are several important macroscopic quantities that are associated with the stellar distribution function, including

* Corresponding author. Present address: Department of Mathematics, Michigan State University, East Lansing, MI 48824, USA. Tel.: +1 517 353 6332; fax: +1 517 432 1562.

E-mail addresses: ycheng@math.utexas.edu (Y. Cheng), gamba@math.utexas.edu (I.M. Gamba).

[1] Tel.: +1 512 471 7422; fax: +1 512 471 8694.

1007-5704/$ - see front matter © 2011 Elsevier B.V. All rights reserved.
doi:10.1016/j.cnsns.2011.10.004

$$\text{density} \quad \rho(x,t) = \int_{\mathbb{R}^n} f(x,v,t)dv$$

$$\text{current density} \quad j(x,t) = \int_{\mathbb{R}^n} vf(x,v,t)dv$$

$$\text{kinetic energy} \quad \xi_k(x,t) = \frac{1}{2}\int_{\mathbb{R}^n} |v|^2 f(x,v,t)dv$$

$$\text{gravitational energy} \quad \xi_e(x,t) = -\frac{1}{2}|E(x,t)|^2$$

$$\text{entropy} \quad S = -\int_{\Omega} f\ln(f)dxdv$$

$$\text{enstrophy} \quad I_2 = \int_{\Omega} f^2 dxdv,$$

$$\text{total energy} \quad \int_{\Omega_x} (\xi_k(x,t) + \xi_e(x,t))dx = \int_{\Omega} f\left(\frac{v^2}{2} + \Phi\right)dxdv.$$

The VP Eq. (1) conserves the mass, momentum, energy, entropy, enstrophy and total energy of the system. More importantly, if the initial f is a perturbation around the Maxwellian equilibrium distribution

$$f_{eq} = \frac{\rho_0}{(2\pi\sigma^2)^{n/2}} e^{-\frac{1}{2}v^2/\sigma^2},$$

then by *Jeans swindle* after Sir James Jeans, one can obtain the *Jeans wavenumber*

$$k_J = (4\pi G\rho_0/\sigma^2)^{1/2}$$

and the *Jeans length* $\lambda_J = 2\pi/k_J$. For any initial state $f(x,v,0) = f_{eq}(1 + A\cdot p(k\,x))$, where $p(\cdot)$ is an analytic $2\pi-$ periodic function, if $\lambda > \lambda_J$ or $k < k_J$, the perturbation is unstable and the phenomenon is called the *Jeans instability*. Damping of the perturbation should occur only at wavelengths smaller than the Jeans length. This behavior differs significantly from the electrostatic VP equations for collisionless plasmas, where damping should be expected for all wavenumbers under suitable assumptions on the equilibrium velocity profile, for which the Debye length is roughly defined in the same way as the Jeans length [23]. The Jeans instability accounts for the solutions of the VP system that are interpreted as the collapse of interstellar gas clouds and subsequent star formation. In this paper, we will perform a numerical study of (1) with perturbations associated with various wavenumbers k for the classical Maxwellian equilibrium.

The VP system with the electrostatic force has been studied extensively for the simulation of collisionless plasmas. Popular numerical approaches include the Particle-In-Cell (PIC) methods [5,21], the Lagrangian particle methods [2], the semi-Lagrangian methods [7] and the Eulerian approaches [15], among many others. For the gravitational case, semi-Lagrangian schemes by Cheng and Knorr [7] have been used to simulate one-dimensional problems [17], spherical stellar systems [18] and stellar disks [24]. An Eulerian code has been used to compute the gravitational collapse of a one-dimensional system in [28].

In this paper, we propose to use discontinuous Galerkin (DG) methods to solve the VP system (1). The original DG method dates back to 1973, and was introduced by Reed and Hill [26] for neutron transport. Cockburn and Shu in a series of papers [13,12,11,10,14] developed the Runge–Kutta DG (RKDG) method for hyperbolic equations. The DG methods have been used to simulate the VP system in plasmas [19] and analysis about its stability, accuracy and conservation are discussed in [20,1]. In [19,20], the Poisson equation is solved by a nonsymmetric interior penalty method (NIPG) method [25]. In [1], for one-dimensional VP systems, the Poisson equation has been discretized by the conforming method, mixed finite element methods, and DG methods including the local DG method, the minimal dissipation DG and LDG methods and hybridizable DG methods. The DG method has also been successfully devised to solve 2D incompressible flow in the vorticity stream-function formulation [22] and later generalized to geophysical fluid equations in [3], in which the Poisson equation is treated by continuous finite element methods to ensure the continuity of the normal velocities.

The scope of this paper is to study the numerical aspects of the DG methods for (1) in the one-dimensional setting for stellar systems. One of the main novelties is that we calculated the BGK mode as a function of the distribution f against the particle's total energy for the gravitational VP system. In our computation, we use the classical representation of the solution by Green's function to compute the 1D Poisson equation, therefore the gravitational field is explicitly given as a function of the numerical density. This guarantees no discretization error from the Poisson equation and let us more accurately investigate our DG solver for the Vlasov equations. For multiple-dimensional applications, a suitable elliptic solver as those in [19,20,1,22,3] should be used. A detailed analysis of the DG methods for VP systems in terms of conservation, numerical recurrence, the impact of using different polynomial spaces, and applications in multi-dimensions could be found in a preprint with Cheng et al. [9].

In this paper, we have used a maximum-principle-satisfying limiter that has been recently proposed by Zhang and Shu in [29] for conservation laws on Cartesian meshes, and later extended on triangular meshes [31]. The resulting scheme preserves positivity of numerical solution and is genuinely high order accurate for arbitrary order of discretization. For a complete review for this method, one can refer to [30].

The rest of the paper is organized as follows: in Section 2, we describe the numerical algorithm. Section 3 is devoted to the simulation results for the case of damping and Jeans instability, respectively. We conclude and provide future work in Section 4.

2. Numerical methods

In this section, we will introduce our numerical approach. For simplicity, the VP system (1) in one-dimension is renormalized as

$$\begin{aligned} &\partial_t f + v\cdot\nabla_x f + E\cdot\nabla_v f = 0 \quad \Omega\times(0,T] \\ &\Delta_x\Phi = \textstyle\int_{\mathbb{R}^n} f dv - 1 \quad \Omega_x\times(0,T] \\ &E = -\nabla_x\Phi \quad \Omega_x\times(0,T] \end{aligned} \tag{2}$$

and without loss of generality, we consider the Maxwellian equilibrium distribution

$$f_{eq} = \frac{1}{\sqrt{2\pi}} e^{-\frac{1}{2}v^2}.$$

Consequently, the Jeans wavenumber is $k_J = 1$. The domain we consider is $\Omega = [0,L]\times[-V_c,V_c]$, where V_c is chosen large enough and may be different for various test cases. The boundary conditions in the x-direction has been assumed to be periodic. The domain Ω is partitioned as follows

$$0 = x_{\frac{1}{2}} < x_{\frac{3}{2}} < \cdots < x_{N_x+\frac{1}{2}} = L, \qquad -V_c = v_{\frac{1}{2}} < v_{\frac{3}{2}} < \cdots < v_{N_v+\frac{1}{2}} = V_c.$$

The computational cells are defined as:

$$\begin{aligned} &I_{i,j} = \left[x_{i-\frac{1}{2}}, x_{i+\frac{1}{2}}\right]\times[v_{j-\frac{1}{2}}, v_{j+\frac{1}{2}}], \\ &J_i = [x_{i-1/2}, x_{i+1/2}], \quad K_j = [v_{j-1/2}, v_{j+1/2}] \quad i = 1,\ldots,N_x, \quad j = 1,\ldots,N_v, \end{aligned}$$

where $x_i = \frac{1}{2}\left(x_{i-\frac{1}{2}} + x_{i+\frac{1}{2}}\right)$, and $v_j = \frac{1}{2}(v_{j-1/2} + v_{j+1/2})$ are center points of the cells. We have used a mesh that is the tensor product of the mesh in the x and v direction, because this makes the implied mesh and space for the Poisson equation simple to compute.

For all macroscopic quantities, we use the piecewise polynomial space in the x-direction

$$Z_h^k = \{\xi : \xi|_{J_i} \in P^k(J_i), \quad i = 1,\ldots N_x\}, \tag{3}$$

where $P^k(J_i)$ is the space of polynomials of degree up to k on J_i. For the full (x, v) space, we define

$$V_h^k = \{\varphi : \varphi|_{I_{i,j}} \in \mathbb{P}^k(I_{i,j}), \quad i = 1,\ldots N_x, \quad j = 1,\ldots N_v\} \tag{4}$$

where

$$\mathbb{P}^k(I_{i,j}) = span\{x^l\ v^m, \forall\ 0 \leqslant l+m \leqslant k, l \geqslant 0, m \geqslant 0\} \text{ on } I_{i,j}.$$

We start by reviewing the semi-discrete DG scheme formulation for the Vlasov equation. We find $f_h(x,t) \in V_h^k$, such that

$$\begin{aligned} &\int_{I_{i,j}} (f_h)_t \varphi_h dx dv - \int_{I_{i,j}} v f_h (\varphi_h)_x dx dv + \int_{K_j} \left(\widehat{vf_h}\varphi_h^-\right)_{i+1/2,v} dv - \int_{K_j} \left(\widehat{vf_h}\varphi_h^+\right)_{i-1/2,v} dv - \int_{I_{i,j}} E_h f_h (\varphi_h)_v dx dv \\ &\quad + \int_{J_i} \left(\widehat{E_h f_h}\varphi_h^-\right)_{x,j+1/2} dx - \int_{J_i} \left(\widehat{E_h f_h}\varphi_h^+\right)_{x,j-1/2} dx = 0 \end{aligned} \tag{5}$$

holds for any test function $\varphi_h(x,t) \in V_h^k$. Here and below, we use the following notations $(\varphi_h)^{\pm}_{i+1/2,v} = \lim_{\epsilon\to 0}\varphi_h(x_{i+1/2}\pm\epsilon, v)$, and $(\varphi_h)^{\pm}_{x,j+1/2} = \lim_{\epsilon\to 0}\varphi_h(x, v_{j+1/2}\pm\epsilon)$. $\widehat{vf_h}$ are numerical fluxes. We can assume that in each K_j, v holds constant sign by properly partitioning the mesh. We can then use the upwind flux, which is defined as

$$\widehat{vf_h} = \begin{cases} vf_h^- & \text{if} \quad v \geqslant 0 \quad \text{in} \quad K_j \\ vf_h^+ & \text{if} \quad v < 0 \quad \text{in} \quad K_j \end{cases}. \tag{6}$$

and

$$\widehat{E_h f_h} = \begin{cases} E_h f_h^- & \text{if} \quad \int_{J_i} E_h dx \leqslant 0 \\ E_h f_h^+ & \text{if} \quad \int_{J_i} E_h dx > 0 \end{cases}. \tag{7}$$

The above description coupled with a suitable time discretization, e.g. the TVD Runge–Kutta method [27] will complete the RKDG methods. In this paper, we have used the third order TVD Runge–Kutta method [27] in our simulations. Next, we will describe the positivity-preserving schemes, for more details about the implementations of the scheme, one can refer to [30,8].

In each of the forward Euler step of the Runge–Kutta time discretization, the following procedures are performed:

- On each cell $I_{i,j}$, evaluate $T_{i,j} = \min_{(x,v)\in S_{i,j}} f_h(x,v)$, where $S_{i,j} = \left(S_i^x \otimes \widehat{S}_j^y\right) \bigcup \left(\widehat{S}_i^x \otimes S_j^y\right)$, and S_i^x, S_j^y denote the $(k+1)$ Gauss quadrature points, while $\widehat{S}_i^x, \widehat{S}_j^y$ denote the $(k+1)$ Gauss–Lobatto quadrature points.
- Compute $\widetilde{f}_h(x,v) = \theta(f_h(x,v) - (\overline{f}_h)_{i,j}) + (\overline{f}_h)_{i,j}$, where $(\overline{f}_h)_{i,j}$ is the cell average of f_h on $I_{i,j}$, and $\theta = \min\{1, |(\overline{f}_h)_{i,j}|/|T_{i,j} - (\overline{f}_h)_{i,j}|\}$. This limiter has the effect of keeping the cell average and "squeeze" the function to be positive at points in $S_{i,j}$.
- Use $\widetilde{f}_h$ instead of f_h to update the Euler forward step.

In order to obtain E_h at each time step, we need to solve the Poisson equation numerically. Recall that beyond periodicity, we need to enforce some additional conditions to uniquely determine Φ. For example, we require $\Phi(0,t) = 0$. In the one-dimensional setting, the exact solution can be then obtained by using the fact that $\Phi(0) = \Phi(L)$ as

$$\Phi_h = \int_0^x \int_0^s \rho_h(z,t)dz\, ds - \frac{x^2}{2} - C_E x,$$

where $C_E = -\frac{L}{2} + \frac{1}{L}\int_0^L \int_0^s \rho_h(z,t)dz\, ds$, and

$$E_h = -(\Phi_h)_x = C_E + x - \int_0^x \rho_h(z,t)dz. \tag{8}$$

From (8), we can see that if $f_h \in V_h^k$, then $\rho_h = \int_{-V_c}^{V_c} f_h dv \in Z_h^k$, hence $E_h \in Z_h^{k+1} \bigcap C^0$. This formula uses the classical representation of the solution by Green's function, and is only valid in the one-dimensional setting as mentioned in the introduction. For multiple-dimensions, a suitable elliptic solver needs to be implemented.

3. Numerical results

In this section, we collect simulation results for (2) with various wavenumbers. The critical Jeans wavenumber in (2) is $k_J = 1$. The initial condition is $f(x,v,0) = f_{eq}(1 + A\cos(kx))$. The computational domain is taken as $x \in [0, L = 2\pi/k]$, $v \in [-V_c, V_c]$. From a classical calculation of the linear theory [16], we can derive the dispersion relation as

$$\varepsilon(k,\omega) = 1 - \frac{1}{k^2}\left\{1 + \frac{\omega}{\sqrt{2}k} Z\left(\frac{\omega}{\sqrt{2}k}\right)\right\}, \tag{9}$$

where the plasma $Z-$ function is defined as

$$Z(z) = \frac{1}{\sqrt{\pi}}\int_{-\infty}^{\infty} e^{-t^2}\frac{dt}{t-z} = 2ie^{-z^2}\int_{-\infty}^{iz} e^{-t^2}dt.$$

The relation $\varepsilon(k,\omega) = 0$ will give us a theoretical value of ω when k is known. The imaginary part of ω will be used to benchmark with the damping or growth rate from our numerical results. In all of our simulations, we have used a CFL condition that ensures the stability of the scheme as well as maintains the positivity condition. In particular, for the P^2 space, we have taken $CFL = 0.19$.

3.1. Damping phenomena

In this subsection, we will consider the case of $k/k_J > 1$. We first start with $k/k_J = 2.0$. In this case, the damping is very strong. Here $V_c = 5$ and the perturbation is of magnitude $A = 0.1$. We use P^2 elements and third-order TVD-RK time stepping in the computation. First we use a 100×200 mesh to study the time evolution of the Log Fourier amplitude for gravitational field and density. Here, we assume that, the density can be expanded in the Fourier series $\rho_h(x) = \sum_{n\geqslant 0}\rho_n \cos(nkx)$. The "log Fourier mode" for the gravitational field [19] is defined as $logFM_n(t) = \log_{10}\left(\frac{1}{L}\sqrt{|\int_0^L E_h(x,t)\sin(knx)dx|^2 + |\int_0^L E_h(x,t)\cos(knx)dx|^2}\right)$. The theoretical damping rate calculated from the dispersion relation (9) is -0.187. From Fig. 1, we measure the damping rate for the first mode of density $\rho_1 (0.5 \leqslant t \leqslant 3)$ to be -0.1872, while for $logFM_1$ it measures -0.1871. Both agree with the theoretical prediction and they share similar time behaviors. In Fig. 2, we plot the evolution of the macroscopic quantities. The particle number (mass), momentum and total energy are well conserved. In particular, for a 200×400 mesh, the amount of mass that is lost from $t = 0$ to $t = 130$ is 1.8×10^{-8} of the original mass. The amount of the total energy change for the same period is 4.5×10^{-7} of the original value. In fact, in [9], the authors show that the DG schemes in its present form can preserve mass exactly in fully discrete level, when there is no boundary effect, i.e., when the domain is chosen large enough such that the f vanishes on the phase space boundaries at all times. Here, we can see that the discrepancy is induced by choosing $V_c = 5$, which gives non-zero but very small f at the phase space boundaries.

Fig. 3(a) contains a plot of the BGK mode (i.e., the relationship given by the order pair ($\epsilon = v^2/2 + \Phi(x,T)$, $f(x,v,T)$)) at $T = 100$. In Fig. 3(b), we have seen the system has almost reached at steady state at $T = 100$. In Fig. 3(c) and (d), we show

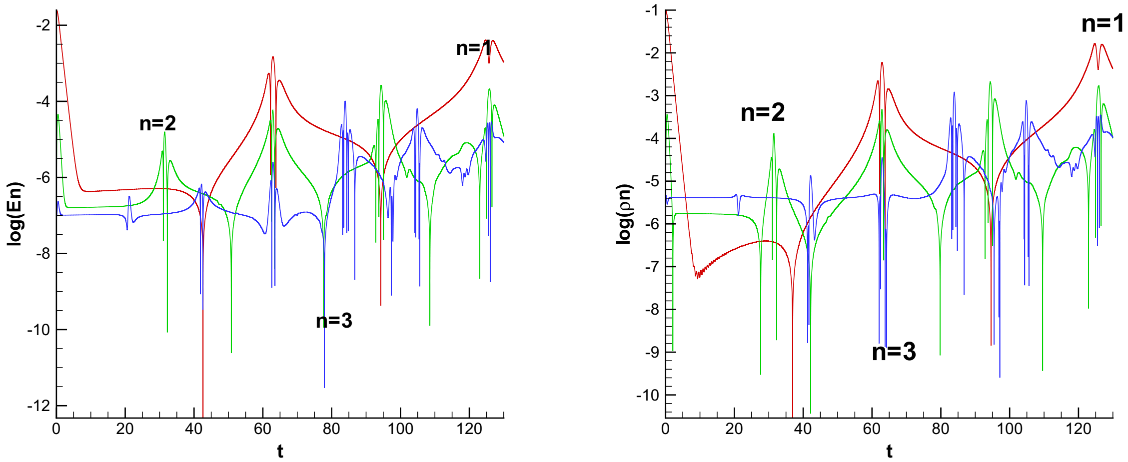

(a) Plot of the first three log Fourier modes ($n = 1, 2, 3$) for the gravitational field $E(x)$ as a function of time

(b) Log Plot of the first three Fourier amplitudes ($n = 1, 2, 3$) for the density $\rho(x)$ as a function of time.

Fig. 1. Damping with $k/k_J = 2.0$ and $A = 0.1$. P^2 elements and third-order TVD-RK time stepping on a 100×200 mesh.

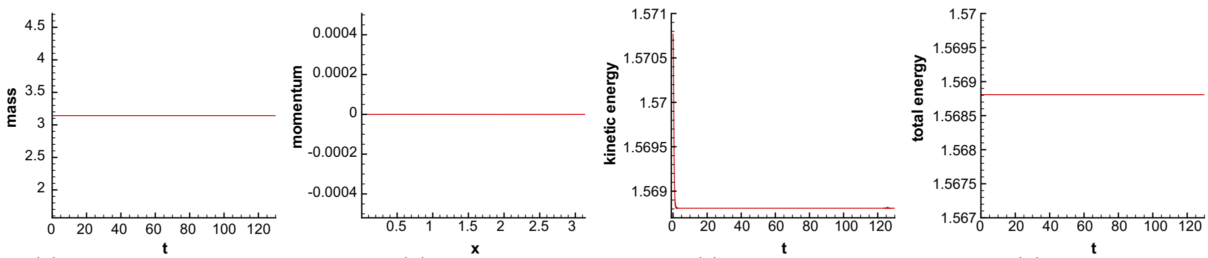

(a) total particle number (b) momentum (c) kinetic energy (d) total energy

Fig. 2. Damping with $k/k_J = 2.0$ and $A = 0.1$. Evolution of macroscopic quantities. P^2 elements and third-order TVD-RK time stepping on a 200×400 mesh.

the details of the BGK plots at $T = 100, 120, 130$. The plots demonstrate an interesting bar type structure with shorter bars near the tail. As time progresses, the height of the bars is reduced (see Fig. 3(c)). This verifies the convergence of the BGK modes to a single-valued discrete function as $t \to \infty$. We also remark that the distance between those bars are mesh size dependent, but time independent.

Next, we consider $k/k_J = 1.1$, $V_c = 5$, $A = 0.1$. For a 200×400 mesh, the numerical damping rate for $\rho_1 (1 \leqslant t \leqslant 4)$ is -0.1621, while for $logFM_1 (1 \leqslant t \leqslant 4)$ it is -0.1620, which agrees with theoretical rate calculated from the dispersion relation (9), -0.163. In Fig. 4, we plot the evolution of the macroscopic quantities. The ratio of mass change from $t = 0$ to $t = 100$ is 1.4×10^{-7}, and it is 3.4×10^{-6} for the total energy. From the momentum plot Fig. 5(b), we can identify that the system is close to but not yet at steady state. This fact can seen from the close up plots Fig. 5(c) and (d), in which detailed structures of the mode can be observed.

3.2. The Jeans instability

In this subsection, we consider the Jeans instability case with $k/k_J < 1$. We consider the weak Jeans instability with $k/k_J = 0.8$, $A = 0.01$, and $V_c = 5$; as well as the strong Jeans instability, $k/k_J = 0.1$, $A = 0.01$, and $V_c = 35$. The computations are performed with P^2 elements and third-order TVD-RK time stepping on a 200×400 mesh. For the weak Jeans instability, the ratio of mass change from $t = 0$ to $t = 100$ is 0.82×10^{-6}, and it is 2.07×10^{-5} for the total energy. For the strong Jeans instability, unlike all previous cases, the total energy is not well conserved with the positivity-preserving limiter. We believe this is due to the strong instability of the problem. We choose to use the RKDG scheme without the positivity-preserving limiter only for this example. In Fig. 6, we plot the evolution of ρ_1 for both cases. The growth rate for $\rho_1 (1 \leqslant t \leqslant 4)$ is 0.3048 for the weak Jeans instability, and it is 0.9764 for the strong case ($2 \leqslant t \leqslant 4$). Those agree with

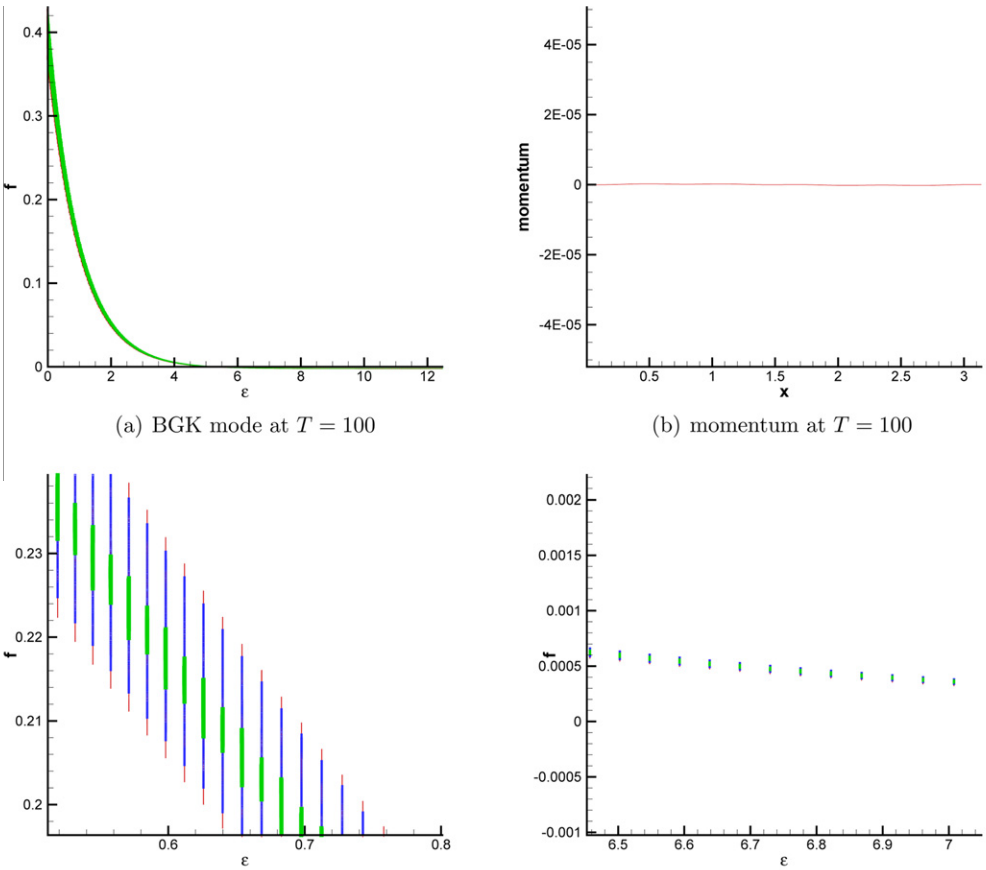

(a) BGK mode at $T = 100$

(b) momentum at $T = 100$

(c) magnified plot of BGK mode at $T = 100, 120, 130$. red: $T = 100$, blue, $T = 120$, green, $T = 130$

(d) magnified plot of BGK mode $T = 100, 120, 130$. red: $T = 100$, blue, $T = 120$, green, $T = 130$

Fig. 3. Damping with $k/k_J = 2.0$ and $A = 0.1$. P^2 elements and third-order TVD-RK time stepping on a 200×400 mesh. (For interpretation of the references to colour in this figure legend, the reader is referred to the web version of this article.)

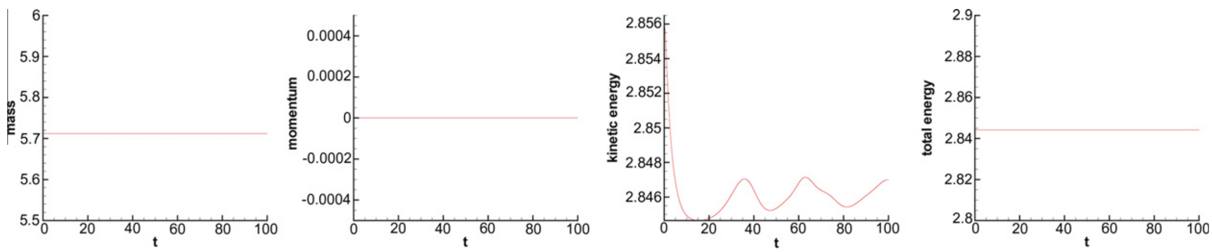

(a) total particle number

(b) momentum

(c) kinetic energy

(d) total energy

Fig. 4. Damping with $k/k_J = 1.1$ and $A = 0.1$. Evolution of macroscopic quantities. P^2 elements and third-order TVD-RK time stepping on a 200×400 mesh.

theoretical rate from the dispersion relation (9), 0.304 and 0.985, resp. After saturation, we can see that ρ_1 undergoes oscillations that eventually damp. In Fig. 7(a), we plot the BGK mode at $T = 100$ for the weak Jeans instability. It clearly does not form a curve because the system is not in equilibrium, see Fig. 7(b) for verification. The contour plots of the *pdf* $f(x, v, t)$ at various times can be found in Figs. 8 and 9. For the strong Jeans instability, we can see that the distribution is first distorted and then develops a core-halo structure similar to the corresponding one in [17] for the same choice of wavenumber and amplitude of perturbation.

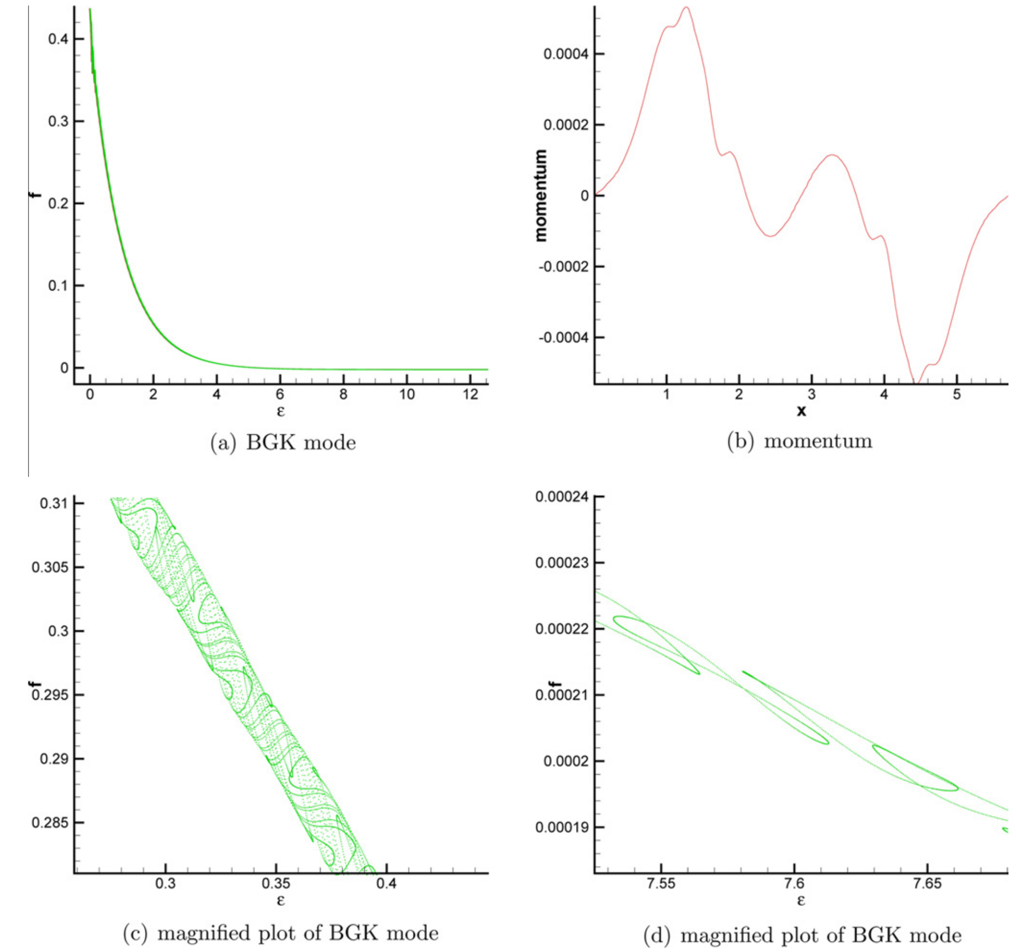

(a) BGK mode (b) momentum

(c) magnified plot of BGK mode (d) magnified plot of BGK mode

Fig. 5. Damping with $k/k_J = 1.1$ and $A = 0.1$ at $T = 100$. P^2 elements and third-order TVD-RK time stepping on a 200×400 mesh.

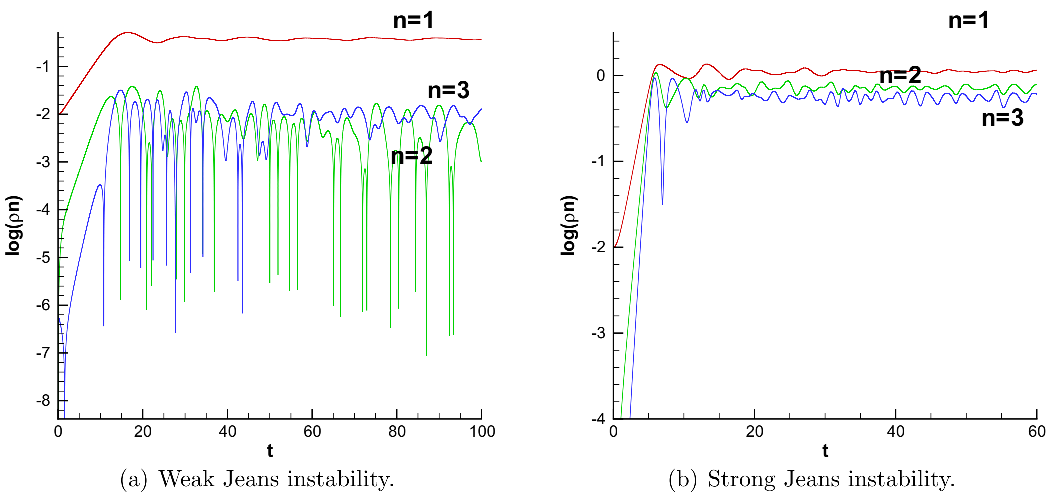

(a) Weak Jeans instability. (b) Strong Jeans instability.

Fig. 6. Jeans instability. Log Plot of the first three Fourier amplitudes ($n = 1,2,3$) for the density $\rho(x)$ as a function of time. P^2 elements and third-order TVD-RK time stepping on a 200×400 mesh.

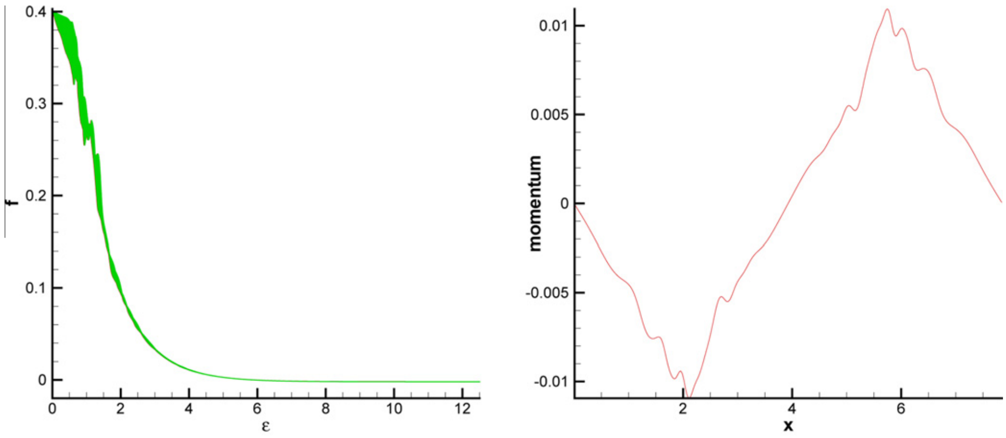

(a) BGK mode (b) momentum

Fig. 7. Weak Jeans instability. P^2 elements and third-order TVD-RK time stepping on a 200×400 mesh.

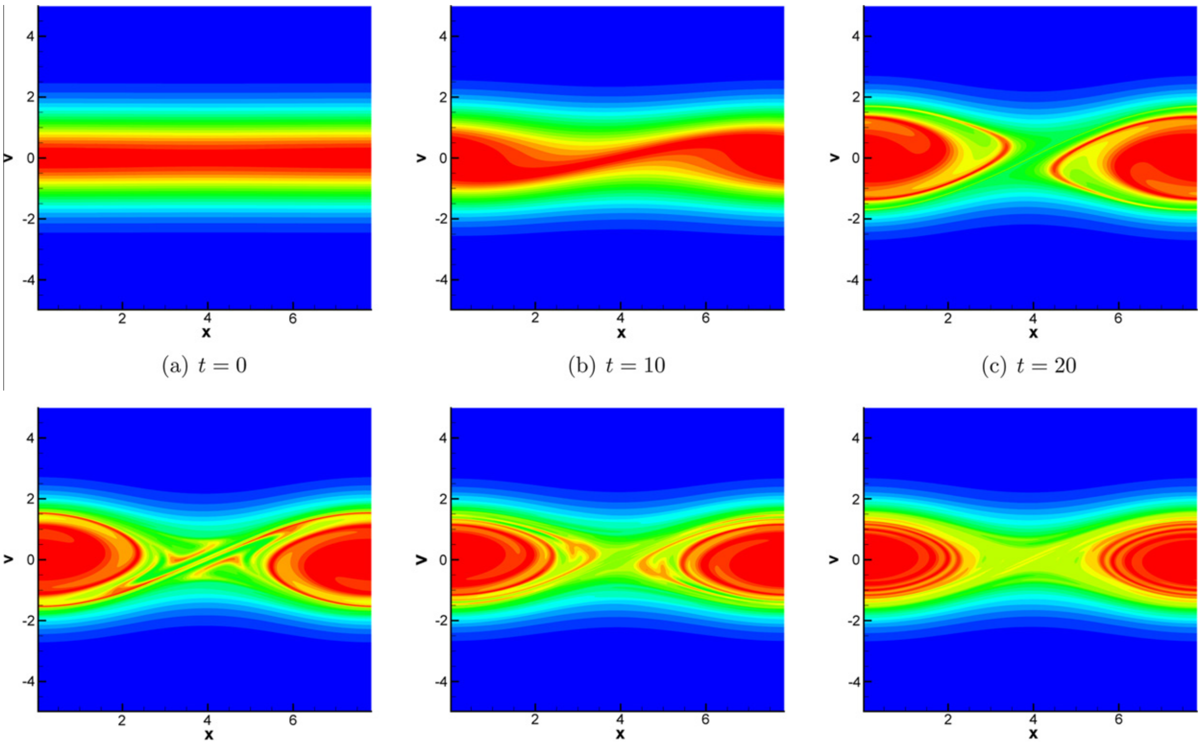

(a) $t = 0$ (b) $t = 10$ (c) $t = 20$

(d) $t = 30$ (e) $t = 50$ (f) $t = 100$

Fig. 8. Weak Jeans instability. Contour plots of *pdf* at various times. P^2 elements and third-order TVD-RK time stepping on a 200×400 mesh.

4. Conclusions and future work

In this paper, we used a high-order discontinuous Galerkin scheme to compute the gravitational Vlasov–Poisson equations. The scheme was stable, accurate and conservative. We compute the case of damping and the Jeans instability with the initial condition taken as a perturbation of the Maxwellian distribution. Future work includes a detailed study of the Jeans instability with multi-bump (two-streaming) distributions, and comparison with the fluid theory [6].

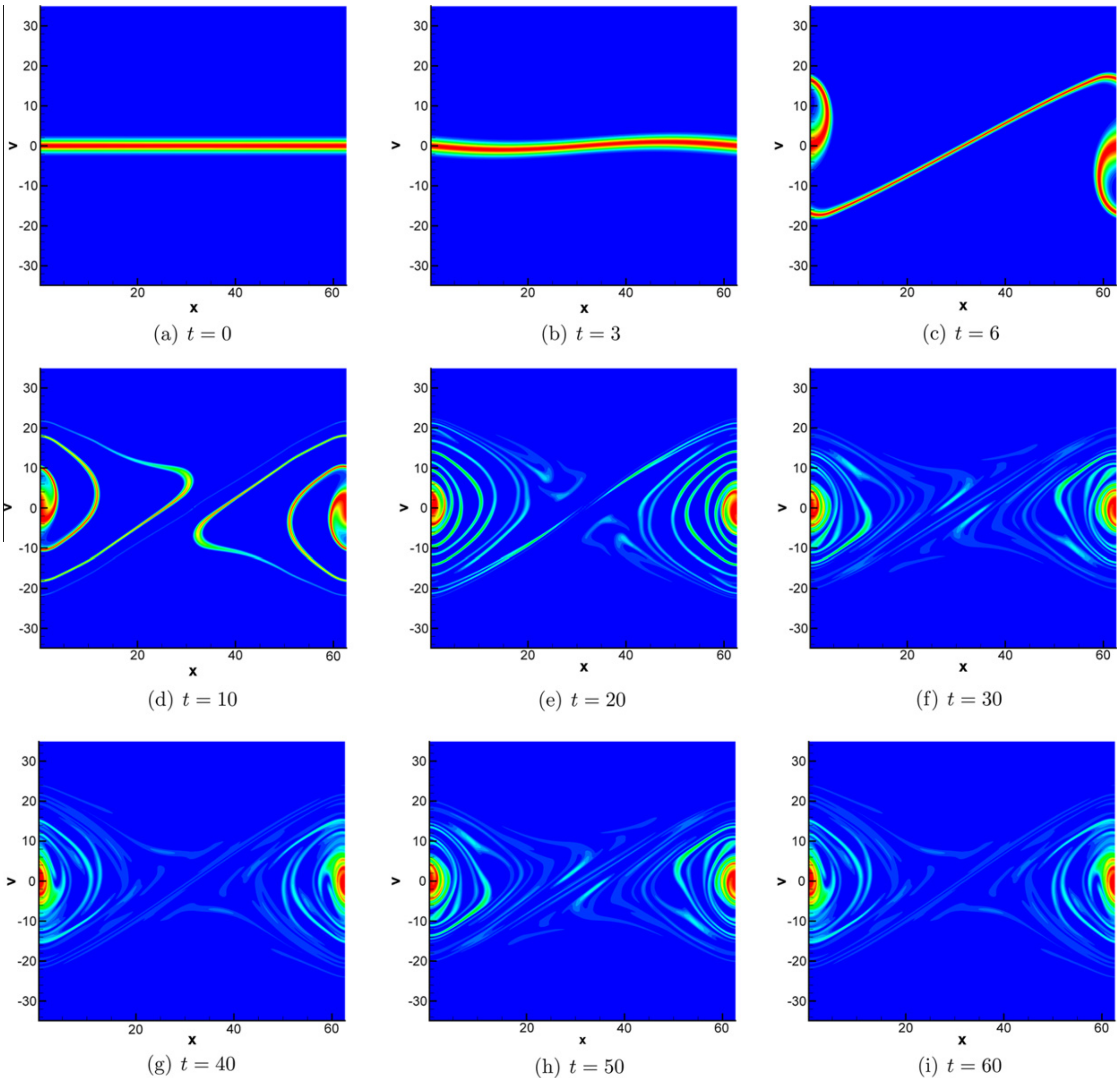

Fig. 9. Strong Jeans instability. Contour plots of *pdf* at various times. P^2 elements and third-order TVD-RK time stepping on a 200×400 mesh.

Acknowledgments

The authors thank Philip J. Morrison for many helpful and illuminating discussions. Yingda Cheng is supported by grant NSF DMS-1016001. Irene M. Gamba is supported by grant NSF DMS-0807712 and also DMS-0757450. Support from the Institute of Computational Engineering and Sciences and the University of Texas Austin is gratefully acknowledged.

References

[1] Ayuso B, Carrillo JA, Shu C-W. Discontinuous Galerkin methods for the one-dimensional Vlasov–Poisson system. Kinetic Related Model, to appear.
[2] Barnes J, Hut P. A hierarchical o(n log n) force-calculation algorithm. Nature 1986;324:446–9.
[3] Bernsen E, Bokhove O, van der Vegt JJW. A (Dis)continuous finite element model for generalized 2D vorticity dynamics. J Comput Phys 2006;211(2):719–47.
[4] Binney J, Tremaine S. Galactic dynamics. Princeton Ser Astrophys. Princeton University Press; 2008.
[5] Birdsall CK, Langdon AB. Plasma physics via computer simulation. Institute of Physics Publishing; 1991.
[6] Casti A, Morrison PJ, Spiegel EA. Negative energy modes and gravitational instability of interpenetrating fluids. In: Buchler JR, Gottesman ST, Kandrup HE, editors. Nonlinear Dynam Chaos Astrophys, Vol. 867. Annals of the New York Academy of Sciences; 1998. p. 93C108.
[7] Cheng CZ, Knorr G. The integration of the Vlasov equation in configuration space. J Comput Phys 1976;22(3):330–51.

[8] Cheng Y, Gamba I, Proft J. Positivity-preserving discontinuous Galerkin schemes for linear Vlasov–Boltzmann transport equations. Math Comput 2010. to appear.
[9] Cheng Y, Gamba IM, Morrison PJ. On Runge–Kutta discontinuous Galerkin schemes for Vlasov–Poisson systems, preprint.
[10] Cockburn B, Hou S, Shu C-W. The Runge-Kutta local projection discontinuous Galerkin finite element method for conservation laws IV: the multidimensional case. Math Comput 1990;54:545–81.
[11] Cockburn B, Lin SY, Shu C-W. TVB Runge-Kutta local projection discontinuous Galerkin finite element method for conservation laws III: one dimensional systems. J Comput Phys 1989;84:90–113.
[12] Cockburn B, Shu C-W. TVB Runge-Kutta local projection discontinuous Galerkin finite element method for conservation laws II: general framework. Math Comput 1989;52:411–35.
[13] Cockburn B, Shu C-W. The Runge–Kutta local projection p1-discontinuous Galerkin finite element method for scalar conservation laws. Math Model Num Anal 1991;25:337–61.
[14] Cockburn B, Shu C-W. The Runge–Kutta discontinuous Galerkin method for conservation laws V: multidimensional systems. J Comput Phys 1998;141:199–224.
[15] Filbet F, Sonnendrücker E. Comparison of Eulerian vlasov solvers. Comput Phys Commun 2003;150:247–66.
[16] Fried BD, Conte SD. The plasma dispersion function. London: Academic Press; 1961.
[17] Fujiwara T. Vlasov simulations of stellar systems: infinite homogeneous case. Astron Soc Japan Publications 1981;33:531–40.
[18] Fujiwara T. Integration of the collisionless Boltzmann equation for spherical stellar systems. Astron Soc Japan Publications 1983;35:547–58.
[19] Heath RE, Gamba IM, Morrison PJ, Michler C. A discontinuous Galerkin method for the Vlasov–Poisson system. J Comput Phys 2011. to appear.
[20] Heath RE. Numerical analysis of the discontinuous Galerkin method applied to plasma physics. Ph.D. dissertation, The University of Texas at Austin, 2007.
[21] Hockney RW, Eastwood JW. Computer simulation using particles. New York: McGraw-Hill; 1981.
[22] Liu J-G, Shu C-W. A high-order discontinuous Galerkin method for 2D incompressible flows. J Comput Phys 2000;160(2):577–96.
[23] Mouhot C, Villani C. On Landau damping. Acta Math 2011. to appear.
[24] Nishida MT, Watanabe Y, Fujiwara T, Kato S. Collisionless Boltzmann simulation of stellar disks: III deformation of spiral normal modes to bar patterns. Astron Soc Japan Publications 1984;36:27–40.
[25] Riviere B, Wheeler MF, Girault V. A priori error estimates for finite elements based on discontinuous approximation spaces for elliptic problems. SIAM J Numer Anal 2001;39:902–31.
[26] Reed W, Hill T. Tiangular mesh methods for the neutron transport equation. Technical report, Los Alamos National Laboratory, Los Alamos, NM, 1973.
[27] Shu C-W, Osher S. Efficient implementation of essentially non-oscillatory shock-capturing schemes. J Comput Phys 1988;77:439–71.
[28] White RL. A new numerical technique for calculation of phase space evolution of stellar systems. The Use Supercomput Stellar Dynam 1986;267:167–74. Lecture Notes in Physics.
[29] Zhang X, Shu C-W. On maximum-principle-satisfying high order schemes for scalar conservation laws. J Comput Phys 2010;229:3091–120.
[30] Zhang X, Shu C-W. Maximum-principle-satisfying and positivity-preserving high order schemes for conservation laws: Survey and new developments. In: Proc Royal Soc A. 2011.
[31] Zhang X, Xia Y, Shu C-W. Maximum-principle-satisfying and positivity-preserving high order discontinuous Galerkin schemes for conservation laws on triangular meshes. J Sci Comput, to appear.